J. Fluid Mech. (1991), *vol.* 229, *pp.* 483–497
Printed in Great Britain

Novel bifurcation phenomena in a rotating annulus

By S. J. TAVENER[1], T. MULLIN[2] AND K. A. CLIFFE[3]

[1] Pennsylvania State University, University Park, PA 16802, USA
[2] Clarendon Laboratory, Parks Road, Oxford OX1 3PU, UK
[3] Theoretical Studies Department, Harwell Laboratory, Oxon. OX11 0RA, UK

(Received 21 March 1988 and in revised form 20 October 1990)

We present an experimental and numerical study of a novel variant of the Taylor–Couette problem. The ends of the annular region rotate with the inner cylinder producing a strong, symmetric forcing of the flow. One consequence of the imposed forcing is that *asymmetric* flows are more readily found than in the standard stationary-ends case. This has led to the discovery of several new and interesting bifurcation phenomena, including codimension-two points of a type normally associated with chaos in finite-dimensional dynamical systems.

1. Introduction

The rich variety of bifurcation phenomena that may be observed in Taylor–Couette flow has provided a convenient setting for careful comparison between the results of controlled experiments and numerical solutions of the Navier–Stokes equations (see for example Cliffe & Mullin 1985 and Cliffe 1989). To date, most of the work on the finite-length problem has been concerned with steady bifurcation, although the more recent work of Mullin, Cliffe & Pfister (1987) has dealt with the origins of time-dependence which arises at multiple bifurcation points in the steady solution set. The time-dependent motion thus formed may be either regular or irregular and is found to pervade a wide range of parameter space. This type of periodic motion differs from the so-called wavy Taylor vortices studied by Davey, DiPrima & Stuart (1968), Kreuger, Gross & DiPrima (1966), DiPrima & Grannick (1971), Iooss (1986) and others. For the wide-gap case studied here, the instability leading to wavy Taylor vortices occurs at much higher Reynolds numbers, as shown by the numerical calculations of Jones (1981, 1982, 1985) and the experiments of Mullin & Benjamin (1980), Lorenzen & Mullin (1985) and Mullin (1985).

A prominent feature of the recent investigations is the role played by symmetry-breaking bifurcations. The flows arising at such bifurcation points are no longer mirror symmetric about the mid-plane of the annulus. The symmetry-breaking bifurcation points move around on the symmetric solution surface as the auxiliary (geometric) parameters are varied. They can interact with folds in the symmetric solution set at double singular points. A pair of paths of Hopf bifurcation points, one on each of the two asymmetric surfaces, can sometimes emerge from such a point (Langford 1979; Schaeffer & Golubitsky 1981; Dangelmayr & Armbruster 1983 and Mullin *et al.* 1987). Multiple bifurcation points in problems having a spatial symmetry have been widely studied in recent years. In particular, the Taylor–Couette problem with co-rotating or counter-rotating cylinders and with periodic boundary conditions at the ends of prescribed length of the annulus has been examined by Golubitsky & Stewart (1986), Chossat, Demay & Iooss (1987),

Langford, *et al.* (1988) and Golubitsky & Langford (1988). Their results, however, are not relevant to the present case because the presence of endwalls destroys translational invariance in the axial direction. The symmetries which exist in the physical problem are reflectional symmetry about the mid-plane of the annulus and an azimuthal symmetry, namely the group of rotations about the common axis of the cylinders. The effect of symmetry-breaking bifurcations, when the symmetry is of reflection type, has been studied in the related problem of Taylor vortices in spherical Couette flow by Tuckerman (1983), Schrauf (1986) and Marcus & Tuckerman (1987*a*, *b*).

The present study is an experimental and numerical investigation into the effects of boundary conditions on the bifurcation set. Flow in the annular gap between two concentric cylinders is driven by the rotation of the inner cylinder and both the top and bottom end plates which are rigidly attached to it. Thus the outer wall alone is stationary and the cellular motion has strong symmetric forcing from the rotating end plates. It will be shown that symmetry-breaking bifurcations are, perhaps surprisingly, more readily found in this case than in the more commonly studied case of stationary ends.

The primary flow is defined to be the cellular state that is developed by gradual increases in Reynolds number, R, from small values. In the present configuration it consists of an even number of cells with predominantly outward motion adjacent to the rotating ends. The observations by Burkhalter & Koschmeider (1974) using sudden starts in an apparatus with two rotating ends, and by Cliffe & Mullin (1986) in an apparatus with a single rotating end, suggest that the end cells grow at the expense of the inner cells as R is increased. Thus, for any aspect ratio, we expect that the observable steady solution set will be unique at both small and large values of R and will consist of just two cells in the parameter ranges studied here.

In addition, cells adjacent to the rotating ends are observed always to have a direction of rotation such that there is outward motion along the end walls. In other words, *anomalous* modes as observed by Benjamin & Mullin (1981), which would have at least one inward-spiralling cell, are not expected, and they have not been observed in the present system. Thus the high multiplicity which has previously been associated with Taylor–Couette flows is greatly reduced, and further the only cases of non-uniqueness of steady flows are confined to a narrow band of R.

A finite-element code was used to solve the steady axisymmetric Navier–Stokes equations for the flow in an annular gap, and numerical bifurcation techniques were employed to compute loci of singular points in the steady-solution set. We have concentrated on the exchange of priority between the two-cell and four-cell primary states as the aspect ratio is varied. Limits of stability of the competing flows were measured in carefully controlled experiments and compared with their computed stability limits. Much of the exchange behaviour was computed to occur over a range of 10^{-3} in aspect ratio and 10^{-1} in Reynolds number, so that it could not be observed experimentally. In addition, some of the most interesting behaviour occurs on unstable solution surfaces and is therefore only detectable by computation.

Further work on the interesting dynamics associated with one of the codimension-2 singular points is reported in Mullin, Tavener & Cliffe (1989). There it was found that bands of regular and irregular motion could be entered by either increases or decreases of R along a branch of steady solutions.

An outline of the numerical techniques is presented in §2, and the apparatus and experimental methods are discussed in §3. The results are presented in §4, where a comparison between numerical and experimental results is given. Finally, some

conclusions are drawn in §5, where we also outline ongoing research on the dynamics of the problem.

2. Computational techniques

We consider the steady flow of an incompressible fluid in the annular region between two concentric cylinders of radii r_1^* and r_2^* and length l. A cross-section of the fluid-filled region is shown in figure 1. The flow is driven by the inner cylinder and top and bottom surfaces, which rotate with angular velocity Ω. The outer cylinder alone is stationary.

In cylindrical polar coordinates the Navier–Stokes equations for steady axisymmetric incompressible flow are

$$R\left[u_r\frac{\partial u_r}{\partial r}+u_z\frac{\partial u_r}{\partial z}-\frac{u_\theta^2}{(r+\beta)^2}\right]+\frac{\partial p}{\partial r}-\left[\frac{1}{(r+\beta)}\frac{\partial}{\partial r}\left((r+\beta)\frac{\partial u_r}{\partial r}\right)+\frac{1}{\Gamma^2}\frac{\partial^2 u_r}{\partial z^2}-\frac{u_r}{(r+\beta)^2}\right]=0, \tag{2.1}$$

$$R\left[u_r\frac{\partial u_\theta}{\partial r}+u_z\frac{\partial u_\theta}{\partial z}-\frac{u_r u_\theta}{(r+\beta)^2}\right]-\left[\frac{1}{(r+\beta)}\frac{\partial}{\partial r}\left((r+\beta)\frac{\partial u_\theta}{\partial r}\right)+\frac{1}{\Gamma^2}\frac{\partial^2 u_\theta}{\partial z^2}-\frac{u_\theta}{(r+\beta)^2}\right]=0, \tag{2.2}$$

$$R\left[u_r\frac{\partial u_z}{\partial r}+u_z\frac{\partial u_z}{\partial z}\right]+\frac{1}{\Gamma^2}\frac{\partial p}{\partial z}-\left[\frac{1}{(r+\beta)}\frac{\partial}{\partial r}\left((r+\beta)\frac{\partial u_z}{\partial r}\right)+\frac{1}{\Gamma^2}\frac{\partial^2 u_z}{\partial z^2}\right]=0, \tag{2.3}$$

$$\frac{1}{(r+\beta)}\frac{\partial}{\partial r}[(r+\beta)u_r]+\frac{\partial u_z}{\partial z}=0. \tag{2.4}$$

In these equations the following non-dimensional quantities have been introduced:

$$r=\frac{r^*}{d}-\beta, \quad z=\frac{z^*}{l},$$

where

$$\beta=\frac{r_1^*}{d}, \quad d=r_2^*-r_1^*;$$

and

$$(u_r,u_\theta,u_z)=\frac{1}{r_1^*\Omega}\left(u_r^*,u_\theta^*,\frac{u_z^*}{\Gamma}\right), \quad p=\frac{dp^*}{\mu r_1^*\Omega}. \tag{2.5}$$

Here the starred symbols represent the respective dimensional variables and μ is the molecular viscosity. The Reynolds number R and aspect ratio Γ are defined by

$$R=\frac{\Omega r_1^* d}{\nu}, \quad \Gamma=\frac{l}{d}. \tag{2.6}$$

Here ν is the kinematic viscosity of the fluid. Equations (2.1)–(2.4) hold in the region

$$D=\{(r,z):0\leqslant r\leqslant 1, \quad -0.5\leqslant z\leqslant 0.5\}. \tag{2.7}$$

The conditions at the boundary of D are

$$\left.\begin{aligned} &u_r=u_z=0 \quad \text{on} \quad r=0,1 \quad \text{and on} \quad z=\pm\tfrac{1}{2},\\ &u_\theta=\begin{cases}1 & \text{on } r=0,\\ 0 & \text{on } r=1,\\ F(r) & \text{on } z=\pm\tfrac{1}{2},\end{cases}\end{aligned}\right\} \tag{2.8}$$

where $F(r)$ is as shown in figure 2. The form of F corresponds to a rigid-body rotation

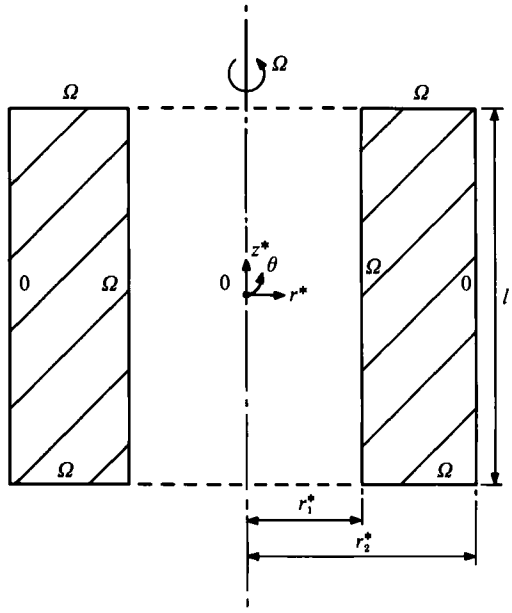

FIGURE 1. Cross-section through flow configuration showing rotating ends and local coordinate system.

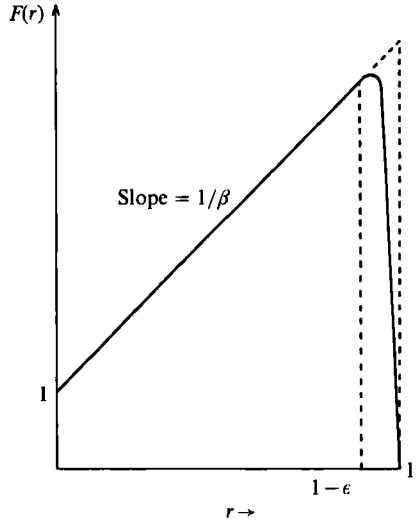

FIGURE 2. Azimuthal velocity boundary condition at $z = \pm\frac{1}{2}$.

up to a distance ϵ from the outer cylinder. Over the small distance ϵ a quadratic variation is used matching the value and slope of the rigid body rotation at $r = 1-\epsilon$ and being zero at $r = 1$. This assumption corresponds to the interpolation scheme used for the azimuthal component of velocity (see below). It is clear that the azimuthal velocity in the experiment must behave in a similar way although the exact form of F is unknown. Our experience is that, provided ϵ is sufficiently small (<0.02), the effect of the form of F on the flow patterns away from the immediate vicinity of the corners is negligibly small.

As a starting point for the discretization, the Navier–Stokes equations are converted into a nonlinear operator equation in an appropriate Hilbert space. Each

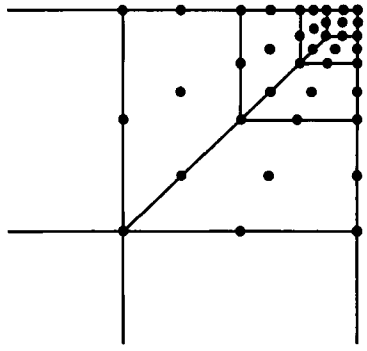

FIGURE 3. Grid refinement at the outer corners.

of the velocity components u_r, u_θ and u_z is required to lie in $W^{1,2}(D)$, the space of functions whose first derivatives are square integrable over the domain D. The pressure p is required to lie in $L^2(D)$, the space of functions that are square integrable over D. The Hilbert space $H = W_0^{1,2}(D)^3 \times L^2(D)$, where $W_0^{1,2}(D)^3$ is the space of vector-valued functions which vanish (weakly) on the boundary of D and whose components lie in $W^{1,2}(D)$.

The finite-element method finds an appropriate solution in a finite-dimensional subspace of the Hilbert space H. We define $H_h = W_{h,0} \times M_h$, where spaces $W_{h,0} \subset W_0^{1,2}(D)^3$ and $M_h \subset L^2(D)$. The parameter h is the length of the longest edge of the finite-element mesh. The velocity space $W_{h,0}$ is generated using nine-noded isoparametric quadrilateral elements with biquadratic interpolation. M_h is generated by piecewise linear interpolation on the same elements. Three pressure degrees of freedom, p, p_x and p_y, are associated with the central node. The pressure interpolation is, in general, discontinuous across element boundaries. The domain $D(2.8)$ was discretized using a 50×5 element basic grid, with local refinement at the two outer corners to cope with the rapid variation in the azimuthal velocity as shown in figure 3. The value of ϵ in (2.8) is chosen equal to the length of that side of the corner element which lies on the end plate. Thus the azimuthal velocity profile on the end plates differs from rigid body only over the last element.

The finite-element equations may be written as a set of nonlinear equations for the nodal values; i.e. in terms of a function f: $\mathbb{R}^n \times \mathbb{R}^3 \to \mathbb{R}^n$ we have

$$f(u; R, \Gamma, \eta) = 0, \tag{2.9}$$

where u is the n-vector of nodal freedoms.

The experimental configuration has reflectional symmetry about the mid-plane, and this property is preserved in the discrete system of nonlinear equations provided the mesh is symmetric about the mid-plane. Cliffe & Spence (1986) construct a finite-dimensional symmetry operator $\hat{S} \in \mathbb{R}^n \times \mathbb{R}^n$ such that

$$f(\hat{S}; R, \Gamma, \eta) = \hat{S} f(u; R, \Gamma, \eta), \quad \hat{S} \neq I, \quad (\hat{S})^2 = I. \tag{2.10}$$

Thus f commutes with $\hat{S}$.

The numerical bifurcation techniques used to compute solution branches and loci of singular points have been discussed in detail by a number of authors (e.g. Cliffe & Spence 1986). The methods used are therefore only briefly described here.

The symmetry operator $\hat{S}$ partitions $\mathbb{R}^n$ into a direct sum of symmetric and antisymmetric components: thus

$$\mathbb{R}^n = \mathbb{R}^n_s + \mathbb{R}^n_a,$$

where

$$u \in \mathbb{R}^n_s \text{ if } \hat{S}u = u \quad \text{and} \quad u \in \mathbb{R}^n_a \text{ if } \hat{S}u = -u. \tag{2.11}$$

For sufficiently small Reynolds numbers, the Navier–Stokes equations have a unique solution in a bounded domain (Serrin 1959), and in a symmetric domain this unique solution will be symmetric (Benjamin 1978*a*, *b*). It can be shown that the null eigenvector at a simple singular point $(\boldsymbol{u}_0; R_0, \Gamma, \eta)$, $\boldsymbol{u}_0 \in \mathbb{R}^n_s$, must be either an element of $\mathbb{R}^n_s$ or else an element of $\mathbb{R}^n_a$. If the null eigenvector $\boldsymbol{\phi}_0 \in \mathbb{R}^n_s$, the bifurcation is symmetry-preserving since the bifurcating solutions remain elements of $\mathbb{R}^n_s$. The expected or codimension-one symmetry-preserving singularity is a quadratic turning point. If the null eigenvector $\boldsymbol{\phi}_0 \in \mathbb{R}^n_a$, bifurcating solutions no longer remain elements of $\mathbb{R}^n_s$, and such bifurcations are said to be symmetry-breaking. The codimension-one symmetry-breaking singularity is a pitchfork bifurcation which gives rise to a pair of asymmetric solutions. We note that asymmetric solutions, which are no longer symmetric with respect to reflection about the mid-plane of the annulus, always occur in pairs which have equivalent stability properties and bifurcation points.

Keller arclength continuation (Keller 1977) was used to compute solution branches, and all loci of singular points. This technique preserves the regularity of the system of nonlinear equations at simple turning points.

An extended system developed by Moore & Spence (1980) was used to compute loci of quadratic turning points. Non-degenerate hysteresis points (cubic turning points) may also be computed as regular solutions of the extended system proposed by Spence & Werner (1982). Transcritical bifurcation points and isola formation points were computed using the technique proposed by Spence & Jepson (1984). These points are distinguished by the sign of an expression involving higher-order derivatives.

Werner & Spence (1984) present a method for computing symmetry-breaking bifurcation points as regular solutions of a simple extended system. It is important to note that in calculating symmetry-breaking singular points the symmetry condition can be used to reduce, by approximately half, the number of degrees of freedom in the problem (Cliffe & Spence 1986). This is done, essentially, by discretizing the lower half of the domain D (i.e. $z \leqslant 0$). Of course, a full grid must be used to compute asymmetric solutions. Coalescence points are turning points in paths of symmetry-breaking bifurcation points and may be computed using an extended system given by Cliffe & Spence (1984). Two types of coalescence points exist, depending upon whether the asymmetric surface lies inside the locus of symmetry-breaking bifurcation points (C^+ type) or outside the locus of bifurcation points (C^- type). This distinction can be made on the basis of the sign of an expression involving higher-order derivatives. At quartic bifurcation points the shape of the asymmetric branches is locally quartic rather than quadratic. Quartic bifurcation points necessarily occur if a supercritical symmetry-breaking bifurcation point becomes subcritical (or vice versa) with continuous change in a parameter. Cliffe & Spence (1984) given an extended system for computing quartic bifurcation points. At a double singular point $(\boldsymbol{u}_0; R_0, \Gamma_0, \eta)$, $\boldsymbol{u}_0 \in \mathbb{R}^n_s$, the derivative (f^0_u) has a two-dimensional null space spanned by a symmetric and an antisymmetric eigenvector, i.e. $\boldsymbol{\Phi}^1_0 \in \mathbb{R}^n_s$ and $\boldsymbol{\varphi}^2_0 \in \mathbb{R}^n_a$. Double singular points occur at the non-transversal intersection of a path of quadratic turning points and a path of symmetry-breaking bifurcation points. Werner (1984) gives a method for their computation.

In order to determine the linear stability of a steady asymmetric solution $(\boldsymbol{u}; R, \Gamma, \eta)$ with respect to an axisymmetric time-dependent perturbation of the form $\zeta = \zeta e^{-\gamma t}$ $(\gamma = \sigma + i\omega)$, the time-derivative terms must be incorporated into the weak form of the steady Navier–Stokes equations in (2.9). Discretizing the spatial

dependence only gives rise to a set of ordinary differential equations, for the vector of nodal freedoms, of the form:

$$\boldsymbol{M}\frac{\partial \boldsymbol{u}}{\partial t}+\boldsymbol{f}(\boldsymbol{u};R,\Gamma,\eta)=\boldsymbol{0}, \tag{2.12}$$

where $\boldsymbol{M}$ is the mass matrix, $\boldsymbol{f}(\boldsymbol{u};R,\Gamma\eta)=\boldsymbol{0}$ is the equation (2.9) governing steady axisymmetric solutions, and the nodal freedoms $\boldsymbol{u}$ are continuous functions of time. The stability of steady, axisymmetric solutions to axisymmetric time-dependent disturbances $\boldsymbol{\zeta}$ is determined by solutions of the generalized eigenproblem

$$\boldsymbol{f}_{\boldsymbol{u}}\boldsymbol{\zeta}=\gamma\boldsymbol{M}\boldsymbol{\zeta} \quad (\gamma=\sigma+\mathrm{i}\omega). \tag{2.13}$$

If $\sigma>0$ the solution is stable, and if $\sigma<0$ the solution is unstable. Linear stability analysis fails when the real part of the complex eigenvalue is zero, i.e. when $\sigma=0$. If $\omega\neq 0$, and $\partial\sigma/\partial R\neq 0$ then $(\boldsymbol{u}_0;R_0\,\Gamma,\eta)\in\mathbb{R}^n$ is a Hopf bifurcation point at which there will be loss of stability of the steady solution. A branch of periodic solutions emerges from the Hopf point and is stable if the direction of branching is such that it coexists with the unstable steady solutions. The branch is unstable if it coexists with the stable steady solutions. Hopf bifurcation points may be calculated as regular solutions of an extended system described by Griewank & Reddien (1983). Their scheme also converges to turning points, so that a good initial estimate of the Hopf bifurcation point is essential. Cliffe & Mullin (1986) discuss the relation between Hopf bifurcation and double singular points in the Taylor problem (see also Langford 1979; Schaeffer & Golubitsky 1981; Dangelmayr & Armbruster 1983 and Mullin *et al.* 1987).

In order to perform the linear stability analysis with respect to time-dependent disturbances that are $2m\pi-$periodic in the azimuthal direction, i.e. $\boldsymbol{\zeta}=\boldsymbol{\zeta}\mathrm{e}^{-\gamma t}\mathrm{e}^{\mathrm{i}m\theta}$, where $\gamma=\sigma+\mathrm{i}\omega$ and m a positive integer, the θ-derivative terms must be incorporated into the weak form of the time-dependent Navier–Stokes equations in (2.12). Again we discretize the spatial dependence on r and z only, using the finite-element method. This leads to a set of partial differential equations in t and θ, where the dependent variables are the velocity and pressure degrees of freedom in the r-z discretization. The equations may be written in the form

$$\boldsymbol{M}\frac{\partial \boldsymbol{u}}{\partial t}+\boldsymbol{f}(\boldsymbol{u};R,\Gamma,\eta)+\boldsymbol{g}(\boldsymbol{u},\boldsymbol{u}_\theta,\boldsymbol{u}_{\theta\theta},R,\Gamma,\eta)=\boldsymbol{0}, \tag{2.14}$$

where $\boldsymbol{M}$ is the mass matrix, $\boldsymbol{f}(\boldsymbol{u};R,\Gamma,\eta)=\boldsymbol{0}$ is the equation (2.9) governing steady axisymmetric solutions, $\boldsymbol{g}(\boldsymbol{u},\boldsymbol{u}_\theta,\boldsymbol{u}_{\theta\theta},R,\Gamma,\eta)$ contains terms which are non-zero only when the flow is not azimuthally symmetric, and the nodal variables $\boldsymbol{u}$ are continuous functions of time and of azimuthal coordinate θ. The stability of a steady axisymmetric solution $\boldsymbol{u}$ with respect to non-axisymmetric time-dependent disturbances $\boldsymbol{\zeta}$ is determined by solutions of the generalized eigenproblem

$$(\boldsymbol{f}_{\boldsymbol{u}}+\mathrm{i}m\boldsymbol{g}_{\boldsymbol{u}\theta}-m^2\boldsymbol{g}_{\boldsymbol{u}\theta\theta})\boldsymbol{\zeta}=\gamma\boldsymbol{M}\boldsymbol{\zeta} \quad (\gamma=\sigma+\mathrm{i}\omega). \tag{2.15}$$

Singular points on the asymmetric solution surface for which the generalized eigenvalue $\gamma=\sigma+\mathrm{i}\omega$ is purely imaginary may be computed using a generalization of the Griewank & Reddien technique.

3. Experiments

An experimental rig was constructed with a radius ratio of 0.5 and range of aspect ratio from 0.8 to 4.6. The inner cylinder was machined from brass and the outer

cylinder was a length of precision-bore glass tube. They were mounted concentrically between two milled aluminium plates. Two brass collars, forming top and bottom of the test section, were keyed to the inner cylinder so that they rotated with it. The top collar was split into two and connected by interference fitting a bearing so that the top half remained stationary while the lower portion rotated with the inner cylinder. The height of the lower collar was fixed, while the upper one was adjustable. Precise control of the angular velocity of the inner cylinder and two ends was provided by use of a stepping motor, reduction gear and toothed-belt drive. An oscillator was used to control the stepping motor and its frequency was displayed digitally on an electronic counter. Both cylinders were mounted inside a watertight cabinet through which water at 27.3 °C was circulated by a Haake temperature-control unit. The entire construction was placed inside a cabinet in which the temperature of the air was controlled to 0.1 °C. By these means the temperature of the working fluid was controlled to within ± 0.01 °C.

Steady flows were studied using flow-visualization techniques. Small quantities of a pearly substance (Mearl Corporation Superpearl 100) were added to the fluid. When observed at right angles to a slit of light from a slide projector, the cellular structure was clearly seen. The cell boundaries appeared as fine dark bands and their heights were measured using a travelling telescope. By these means the cellular structure was readily determined and its symmetry could also be checked.

Time-dependent flows were more conveniently detected using laser-Doppler velocimetry to measure the radial velocity at a single point in the flow. This technique also afforded an accurate measurement of their period. High-quality 0.23 ± 0.002 mm polystyrene spheres were introduced into the fluid to improve the scattering of the laser light. The traces of velocity versus time were further analysed by a microprocessor-based correlator, so that the temporal characteristics of the flow could be determined. In addition, the LDV system could be split to check on the phases of the various oscillations, which observation helped determine the azimuthal wavenumber m.

Two types of silicone oil were used. Steady bifurcations were observed using a silicone oil of viscosity 4.52 cS. The frequency and growth rate of the axisymmetric periodic flows was very small when this oil was used, so that reliable detection was difficult. Thus a more viscous silicone oil of viscosity 20.01 cS was used to observe these flows. The viscosities of both oils were measured at 27.3 °C by means of an Ubbelhölde suspended level viscometer.

In order to determine the critical Reynolds number for various phenomena, the angular velocity of the inner cylinder and endwalls was changed in steps of less than 0.5% and the flow allowed to settle between each speed change. The settling time required was determined by repeating this process with increasingly long settling times until repeatable results were achieved.

4. Computational and experimental comparison

Computations performed using the numerical techniques discussed in §2 are reported here and compared with experimental results obtained with the apparatus and procedures outlined in §3. Both computations and experiments were performed at a single radius ratio of 0.5. Aspect ratios studied ranged between 2 and 4.

A unique symmetric steady flow exists for both 'small' and 'large' Reynolds numbers, within an intermediate range there are multiple steady solutions. For aspect ratios investigated here, 'small' means $R < 80$ and 'large' means $R > 300$.

The unique steady axisymmetric flow for large Reynolds numbers has two equally sized cells. This property is in marked contrast with the Taylor problem when the ends are stationary; then at large R the multiplicity of steady solutions can be high (Benjamin & Mullin 1982).

Figure 4 is a sketch of the loci of singular points on the (R, Γ)-plane. The scale of the exchange region in the numerical results is not a convenient one, and we have therefore sketched the singular-point diagram and the accompanying sequence of bifurcation diagrams to highlight the salient features. The actual results numerically determined are present in figure 5, where they are compared with those obtained in the experiment.

In figure 4 (*a*), the solid curve JTHDIL is a locus of quadratic turning points of the symmetric solution surface. There are four codimension-two† singular points along this locus: a transcritical bifurcation point T, a non-degenerate hysteresis point H, a double singular point D, and an isola formation point I. The hysteresis point H and the transcritical bifurcation point T are separated by just 0.15 in Reynolds number and by 5×10^{-5} in aspect ratio. With increasing aspect ratio a closed loop of symmetric four-cell solutions develops from the isola formation point I. The curve JTHDIL can be compared with that for the two-cell to four-cell exchange in the case of stationary ends (Cliffe 1989). In that case there is no isola-formation point and the curve marking the stability of the four-cell secondary flow does not bend round as the aspect ratio is decreased. The hysteresis and transcritical bifurcation points occur at broadly similar values of Reynolds number and aspect ratio, although the hysteresis point occurs at lower values than the transcritical point so that the cusp points down in that case. The major difference, however, is that in the standard case, with stationary ends, the symmetry-breaking bifurcations and the various time-dependent flows do not occur. We note that symmetry-breaking and some time-dependent phenomena occur in the 4-cell to 6-cell exchange in the case of stationary ends (Cliffe 1989; Mullin *et al.* 1987).

The dashed line GQDCK in figure 4 (*a*) is a locus of symmetry-breaking bifurcation points (i.e. the reflectional symmetry about the mid-plane of the annulus is broken at this bifurcation point). There are three codimension-two singular points along this locus: a C^+ type coalescence point C, a double singular point D and a quartic bifurcation point Q. A supercritical and subcritical pair of symmetry-breaking bifurcation points, connected by a pair of asymmetric solutions, develops with increasing aspect ratio from the C^+-type coalescence point.

The supercritical symmetry-breaking bifurcation becomes subcritical for $\Gamma > \Gamma_Q$. The chained line EQ thus represents two coincident paths of folds, one on each of the two asymmetric surfaces, which are the lower limits of stability of the branches emerging from the subcritical bifurcation points which lie along QG. The path of symmetry-breaking bifurcations crosses from one symmetric solution surface to the other by rounding the fold in the symmetric surface at the double singular point D.

† Note that we define the codimension of a bifurcation to be the smallest number of parameters necessary for the bifurcation to appear in a stable or persistent way. This is the standard definition in the literature on dynamical systems (see e.g. Guckenheimer & Holmes 1983, p. 123). The definition of codimension that is used more commonly in the literature on bifurcation theory, (see e.g. Golubitsky & Schaeffer 1985, p. 121) depends on the notion of a distinguished parameter. Here the codimension is the minimum number of parameters required to produce a versal unfolding of the bifurcation. An obvious choice for such a distinguished parameter in the problem studied here is the Reynolds number. We have chosen to adopt the former convention as much of our effort has been focused on the dynamical behaviour near the codimension-two points U and V in figure 5 – see Mullin *et al.* (1989).

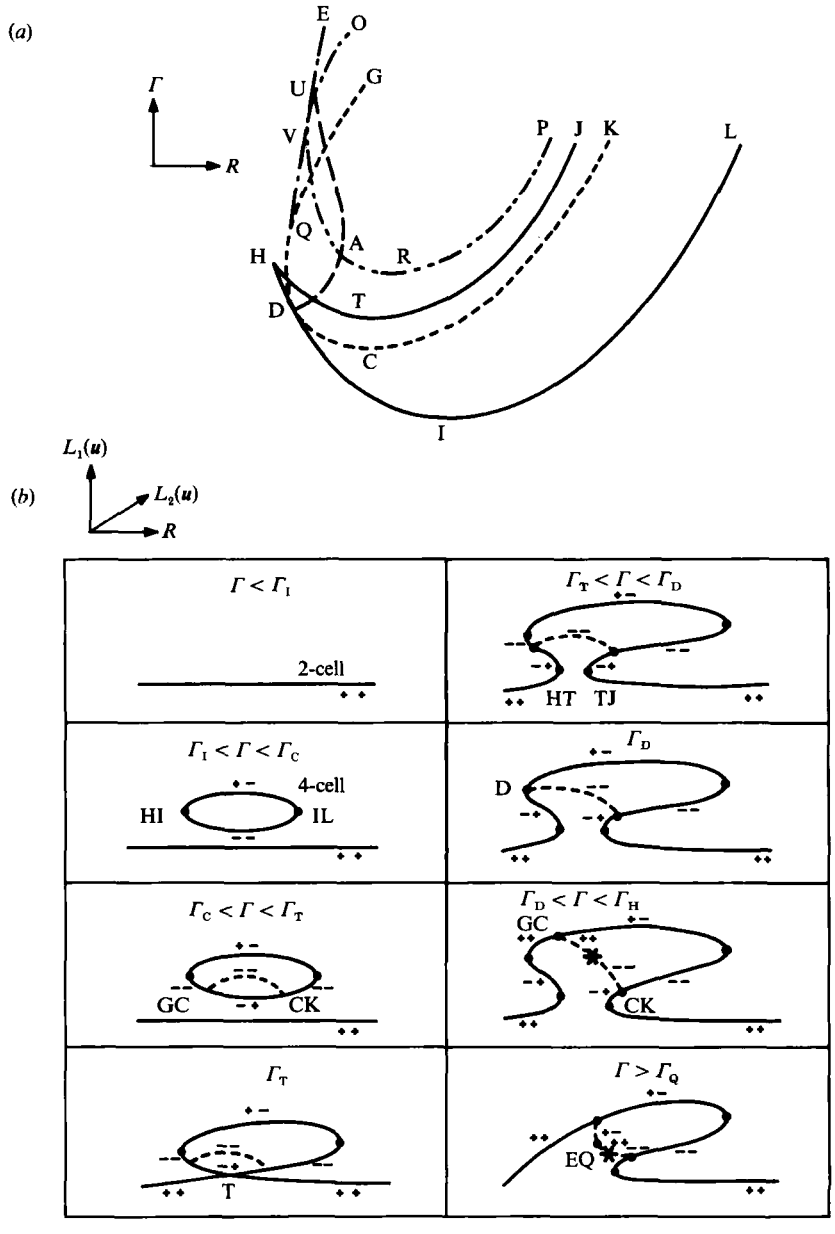

FIGURE 4(*a*) Sketch of the computed loci of singular points for symmetry-preserving and symmetry-breaking, steady bifurcation and for bifurcation to periodic flows. JTHDIL is a path of quadratic turning points, where T is a transcritical bifurcation point, H is a non-degenerate hysteresis or cubic turning point, D is a double singular point and I is an isola formation point. GQDCK is a path of symmetry-breaking bifurcation points, where Q is a quartic bifurcation point and C is a C^+ type coalescence point. EQ represents two paths of quadratic turning points, one on each of the two asymmetric surfaces. DAU represents two paths of axisymmetric ($m = 0$) Hopf bifurcation points, one on each of the two asymmetric surfaces. OVARP represents two paths of non-axisymmetric ($m = 1$) Hopf bifurcation points, one on each of the two asymmetric surfaces. (*b*) Labelling of the singular points of the bifurcation diagrams is consistent with the sketch of the loci of these points in parameter space. Solid branches in the bifurcation diagrams represent symmetric solutions and dashed branches represent asymmetric solutions. Asterisks on the asymmetric branches are ($m = 0$) Hopf bifurcation points.

The locus of symmetry-breaking bifurcations is tangent to the locus of the fold at this point and the null space of the Jacobian f_u is two-dimensional, spanned by a symmetric and an antisymmetric eigenvector. The long-dashed line DAU represents two paths of axisymmetric ($m = 0$) Hopf bifurcation points, one on each of the two asymmetric surfaces. These two paths are coincident at the double singular point D; and the angular frequency, given by the magnitude of the pair of purely imaginary eigenvalues, goes to zero at D. The asymmetric solution surfaces become unstable with respect to axisymmetric periodic flows upon crossing the locus of $m = 0$ Hopf bifurcation points with increasing Reynolds number. The measured frequency of the associated periodic orbits was found to lie between 0.01Ω (near D) and 0.1Ω (close to A). The two paths of Hopf bifurcation points, which originate at D, terminate in a pair of Takens–Bogdanov points marked U in figure 4(*a*).

The dot-dash line OVARP represents two paths of $m = 1$ Hopf bifurcation points, one on each of the two asymmetric surfaces. The two asymmetric surfaces become unstable with respect to a three-dimensional tilt wave, with azimuthal wavenumber $m = 1$, upon crossing VR with increasing Reynolds number. The asymmetric surfaces restabilize with respect to this flow upon crossing RP. Thus, periodic flows with azimuthal wavenumber $m = 1$ exist over a finite range of Reynolds numbers only. There is in effect an isola of $m = 1$ wavy periodic solutions. The frequency of these periodic flows was about 0.23Ω and was essentially independent of R and Γ. Periodic flows with azimuthal wavenumbers of two or more have not been observed either computationally or experimentally.

The sequence of qualitatively different bifurcation diagrams is sketched below the plot of paths of singular points in figure 4(*b*). Bifurcation diagrams are constructed by plotting a linear functional $L_1(\boldsymbol{u})$ of the symmetric component of the solution in one direction (in the plane of the paper), and a linear functional $L_2(\boldsymbol{u})$ of the antisymmetric part of the solution in an orthogonal direction (out of the plane of the paper) against the Reynolds number. The singular points of the bifurcation diagrams are annotated in a way that is consistent with the singular-point diagram. Branch stabilities are determined by evaluating the sign of the symmetric and antisymmetric Jacobian determinants and these are indicated for each branch. The asterisks denote axisymmetric ($m = 0$) Hopf bifurcation points. Index arguments show that the real part of two complex eigenvalues must change sign simultaneously along the asymmetric branches when $\Gamma > \Gamma_{\mathrm{D}}$. This occurs generically at a Hopf bifurcation point where a complex-conjugate pair of eigenvalues cross the imaginary axis. Non-axisymmetric ($m = 1$) Hopf bifurcation points are not shown in order to simplify the presentation.

For $\Gamma < \Gamma_{\mathrm{I}}$, the only solution of equation (2.12) is a symmetric two-cell flow with outwardly spiralling flow along the top and bottom surfaces. When the aspect ratio is increased into the range $\Gamma_{\mathrm{I}} < \Gamma < \Gamma_{\mathrm{T}}$, an isola of symmetric four-cell flows exists, developing from the isola formation point I. The isola of four-cell solutions touches the primary two-cell branch at the transcritical bifurcation point T when $\Gamma = \Gamma_{\mathrm{T}}$. The transcritical bifurcation disconnects in the opposite sense for $\Gamma > \Gamma_{\mathrm{T}}$, and the symmetric two-cell and four-cell solutions constitute part of a single folded branch containing two hysteretic regions. The smaller of these two regions collapses at the non-degenerate hysteresis point H, but the larger hysteresis persists for $\Gamma > \Gamma_{\mathrm{H}}$. Symmetric two-cell and four-cell solutions then lie on a single folded branch. Along this branch the two end-cells grow smoothly and the two middle cells shrink as R is increased, until at sufficiently high values of R the flow has only two cells. This is a smooth process which does not involve any bifurcations.

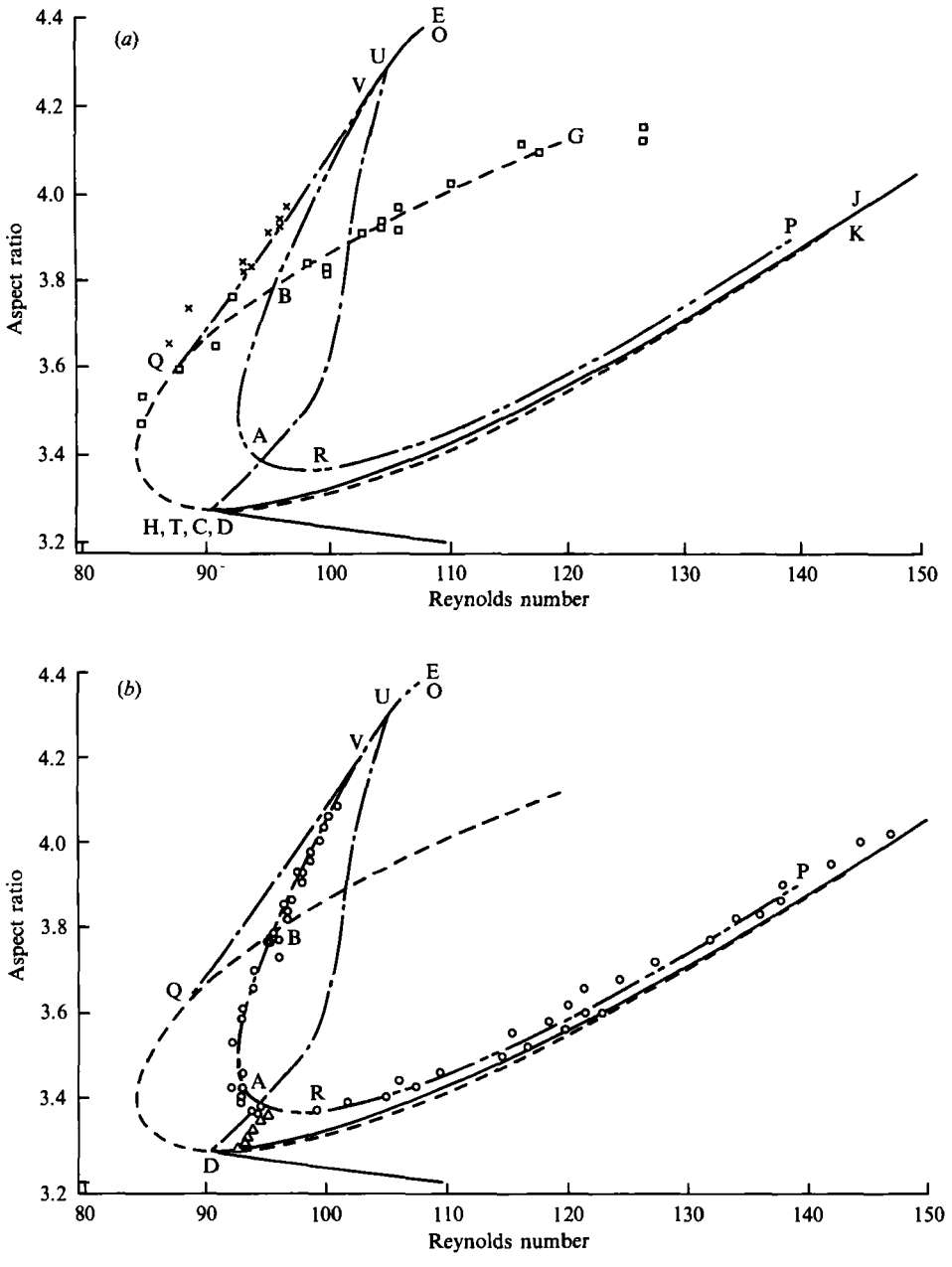

FIGURE 5. Comparison between computed and experimentally determined limits of stability: (*a*) □ experimentally observed symmetry-breaking bifurcation; ×, non-reversible loss of stability of the asymmetric four-cell flow; (*b*) △, Hopf bifurcation to the axisymmetric ($m = 0$) periodic flow; and ○, Hopf bifurcation to the non-axisymmetric ($m = 1$) periodic flow.

In figure 5, experimentally determined stability limits are plotted on the (R, Γ)-plane and compared with the computed loci of codimension-one singularities. Much of the steady bifurcation behaviour is experimentally unobservable. In particular, symmetric and asymmetric four-cell flows are unstable for $\Gamma < \Gamma_D$. The isola-formation and coalescence points I and C and the entire loci DIL and DCK lie on

unstable surfaces and so cannot be detected in experiments. However, we include the loci of the unstable branches since they are essential for a full appreciation of the events observed in the experiment.

The points marked by the squares denote experimentally determined symmetry-breaking bifurcation points, where a marked departure from the symmetric four-cell flow was observed with increasing Reynolds number. The asymmetric flows contained pairs of cells with unequal sizes. The flow with longer cells at the top was generally found more often since presumably small imperfections in the apparatus disconnected the bifurcation in this sense. However, flows with longer cells at the bottom could also be seen, especially if R was varied rapidly in the critical region. Thus the asymmetric flows were due to the presence of a symmetry-breaking bifurcation and were not artifacts of a poorly constructed apparatus.

For $\Gamma_D < \Gamma < \Gamma_Q$ the onset of asymmetry was smooth and reversible, but for $\Gamma_Q < \Gamma < \Gamma_B$ the onset was sudden and exhibited hysteresis. For $\Gamma > \Gamma_B$, the symmetric four-cell flow lost stability suddenly to a periodic flow with $m = 1$. The points marked by crosses show where a catastrophic collapse from the asymmetric solution surface to the symmetric solution surface was observed with decreasing Reynolds number. The points marked by triangles are the experimentally observed $m = 0$ Hopf bifurcation points for the onset of axisymmetric time-dependent flows. Finally, the points marked by circles are the experimentally determined limits of the $m = 1$ isola. Within this region the asymmetric flows were found to become unstable to a three-dimensional tilt wave with wavenumber 1. Far inside this region another more complicated time-dependent motion was also found, as reported in Mullin *et al.* (1989). Agreement between computational and experimental stability limits was achieved to within 2% in all cases.

5. Conclusions

We have presented a study of bifurcation phenomenon in a variant of the Taylor–Couette experiment in which the ends of the annulus rotate with the inner cylinder, the outer being stationary. This configuration produces a driving effect on the end cells which increases with Reynolds number. The result is that all flows, other than the two-cell, tend to lose stability as the Reynolds number increases, essentially because the end cells grow and squeeze out the interior ones. This leads to interesting bifurcation behaviour which is different from that observed in the Taylor experiment with stationary ends.

It is also noteworthy that the strong symmetric driving effect seems to produce asymmetric flows more preferentially than in the case of stationary ends. Symmetry-breaking does play an important role in the case of stationary ends and has a profound effect on the dynamics of the flow (Cliffe & Mullin 1986; Mullin *et al.* 1987); however, it seems to be even more important in the present case.

The study has also revealed a number of codimension-two points with associated interesting dynamical behaviour. While it is possible to write down normal forms which describe the behaviour near the points U and V, the calculation of the required coefficients is a substantial numerical problem in its own right. However, recent extensive experimental studies over these points have uncovered a rich variety of dynamical phenomena which are more complex than can be accounted for by the simple normal forms. It may be that an interaction between U and V (produced by changing the radius ratio) is sufficiently complex to describe the observed phenomena. Some preliminary experimental results on the dynamics near point V in

figures 4 and 5 have been reported by Mullin *et al.* (1989) and Mullin & Price (1989). However, in order to understand the complicated finite-dimensional dynamics of these studies, a full appreciation of the bifurcation structure reflected here is essential.

Finally we re-emphasize the good agreement between the observations and the results of the numerical-bifurcation techniques applied to the finite-element discretization of the Navier–Stokes equations.

We would like to thank Professor T. B. Benjamin for helpful comments on this paper. The research of S.J.T. was supported by a Unilever (NZ) scholarship, T.M. by an SERC Advanced Fellowship and K.A.C. by the Underlying Programme of the UKAEA and by the Royal Society/SERC Industrial Fellowship Scheme. The main part of our programme is supported by the SERC under the Non-linear Initiative.

REFERENCES

BENJAMIN, T. B. 1978*a* Bifurcation phenomena in steady flows of a viscous liquid. Part I: Theory. *Proc. R. Soc. Lond.* A**359**, 1–26.

BENJAMIN, T. B. 1978*b* Bifurcation phenomena in steady flows of a viscous liquid. Part II: Experiments. *Proc. R. Soc. Lond.* A**359**, 27–43.

BENJAMIN, T. B. & MULLIN, T. 1981 Anomalous modes in the Taylor experiment. *Proc. R. Soc. Lond.* A**377**, 221–249.

BENJAMIN, T. B. & MULLIN, T. 1982 Notes on the multiplicity of flows in the Taylor experiment. *J. Fluid Mech.* **121**, 219–230.

BURKHALTER, J. E. & KOSHCHMEIDER, E. L. 1974 Steady supercritical Taylor vortices after sudden starts. *Phys. Fluids* **17**, 1929–1935.

CHOSSAT, P. DEMAY, Y. & IOOSS, G. 1987 Interactions des modes azimutaux dans le probleme de Coutte–Taylor. *Arch. Rat. Mech. Anal.* **99**, 213–248.

CLIFFE, K. A. 1989 Numerical calculations of the primary-flow exchange process in the Taylor problem. *J. Fluid Mech.* **197**, 57–79.

CLIFFE, K. A. & MULLIN, T. 1985 A numerical and experimental study of anomalous modes in the Taylor experiment. *J. Fluid Mech.* **153**, 243–258.

CLIFFE, K. A. & MULLIN, T. 1986 A numerical and experimental study of the Taylor problem with asymmetric end conditions. *AERE Harwell Rep.* TP.1179.

CLIFFE, K. A. & SPENCE, A. 1984 The computation of high order singularities in the finite Taylor problem. In *Numerical Methods for Bifurcation Problems* (ed. T. Küpper, H. D. Mittelmann & H. Weber), ISNM 70, pp. 129–144. Birkhäuser.

CLIFFE, K. A. & SPENCE, A. 1986 Numerical calculations of bifurcations in the finite Taylor problem. In *Numerical Methods for Fluid Dynamics, II* (ed. K. W. Morton & M. J. Baines), pp. 155–176. Clarendon.

DANGELMAYR, G. & ARMBRUSTER, D. 1983 Classification of Z_2-equivariant imperfect bifurcations with corank 2. *Proc. Lond. Math. Soc.* (3) **46**, 517–546.

DAVEY, A. DIPRIMA, R. C. & STUART, J. T. 1968 On the instability of Taylor vortices. *J. Fluid Mech.* **31**, 17–52.

DIPRIMA, R. C. & GRANNICK, R. N. 1971 A nonlinear investigation of the stability of flow between counter-rotating cylinders. In *Proc. IUTAM Symp. 1969, Instability of Continuous Systems* (ed. H. Leipholz), pp. 51–60. Springer.

GOLUBITSKY, M. & LANGFORD, W. F. 1988 Pattern formation and bistability in flow between counter-rotating cylinders. *Physica* D**32**, 362–392.

GOLUBITSKY, M. & SCHAEFFER, D. 1985 *Singularities and Groups in Bifurcation Theory*. Springer.

GOLUBITSKY, M. & STEWART, I. N. 1986 Symmetry and stability in Taylor–Couette flow. *SIAM J. Math. Anal.* **17**, 249–288.

GRIEWANK, A. & REDDIEN, G. 1983 The calculation of Hopf points by a direct method. *IMA J. Numer. Anal.* **3**, 295–303.

GUCKENHEIMER, J. & HOLMES, P. 1983 *Non-linear Oscillations, Dynamical Systems and Bifurcations of Vector Fields*. Springer.

IOOSS, G. 1986 Secondary bifurcations of Taylor vortices into wavy inflow or outflow boundaries. *J. Fluid Mech.* **173**, 273–288.

JONES, C. A. 1981 Non-linear Taylor vortices and their stability. *J. Fluid Mech.* **102**, 249–261.

JONES, C. A. 1982 On flow between counter-rotating cylinders. *J. Fluid Mech.* **120**, 433–450.

JONES, C. A. 1985 The transition to wavy Taylor vortices. *J. Fluid Mech.* **157**, 135–162.

KELLER, H. B. 1977 Numerical solutions of bifurcation and non-linear eigenvalue problems. In *Applications of Bifurcation Theory* (ed. P. H. Rabinowitz), pp. 359–384. Academic.

KREUGER, E. R., GROSS, A. & DIPRIMA, R. C. 1966 On the relative importance of Taylor–vortex and non-axisymmetric modes in flow between rotating cylinders. *J. Fluid Mech.* **24**, 521–538.

LANGFORD, W. F. 1979 Periodic and steady-state mode interactions lead to tori. *SIAM J. Appl. Maths* **37**, 22–48.

LANGFORD, W. F., TAGG, R., KOSTELICH, E. J., SWINNEY, H. L. & GOLUBITSKY, M. 1988 Primary instabilities and bicriticality in flow between counter-rotating cylinders. *Phys. Fluids* **31**, 776–785.

LORENZEN, A. & MULLIN, T. 1985 Anomalous modes and finite length effects in Taylor–Couette flow. *Phys. Rev.* A**31**, 3463–3465.

MARCUS, P. S. & TUCKERMAN, L. S. 1987*a* Simulation of flow between concentric rotating spheres. Part 1. Steady states. *J. Fluid Mech.* **185**, 1–30.

MARCUS, P. S. & TUCKERMAN, L. S. 1987*b* Simulation of flow between concentric rotating spheres. Part 2. Transitions. *J. Fluid Mech.* **185**, 31–65.

MOORE, G. & SPENCE, A. 1980 The calculation of turning points of non-linear equations. *SIAM J. Numer. Anal.* **17**, 567–576.

MULLIN, T. 1985 The transition to time-dependence in Taylor–Couette flow. *Phys. Rev.* A**31**, 1216–1218.

MULLIN, T. & BENJAMIN, T. B. 1980 Transition to oscillatory motion in the Taylor experiment. *Nature* **288**, pp. 567–569.

MULLIN, T., CLIFFE, K. A. & PFISTER, G. 1987 Unusual time dependent phenomena in the Taylor-Couette experiment at moderately low Reynolds number. *Phys. Rev. Lett.*, **58**, 2212–2215.

MULLIN, T. & PRICE, T. J. 1989 An experimental observation of chaos arising from the interaction of steady and time-dependent flows. *Nature* **340**, 294–296.

MULLIN, T., TAVENER, S. J. & CLIFFE, K. A. 1989 An experimental and numerical study of a codimension-2 bifurcation in a rotating annulus. *Europhys. Lett.* **8**, 251–256.

SCHAEFFER, D. & GOLUBITSKY, M. 1981 Bifurcation analysis near a double eigenvalue of a model chemical reaction. *Arch. Rat. Mech. Anal.* **75**, 315–347.

SCHRAUF, G. 1986 The first instability in spherical Taylor–Couette flow. *J. Fluid Mech.* **166**, 287–303.

SERRIN, J. 1959 On the stability of viscous fluid flows. *Arch. Rat. Mech. Anal.* **3**, 1–13.

SPENCE, A. & JEPSON, A. D. 1984 The numerical calculation of cusps, bifurcation points and isola formation points in two parameter problems. In *Numerical methods for Bifurcation Problems* (ed. T. Küpper, H. D. Mittelmann & H. Weber), ISNM 70, pp. 502–514. Birkhäuser.

SPENCE, A. & WERNER, B. 1982 Nonsimple turning points and cusps. *IMA J. Numer. Anal.* **2**, 413–427.

TUCKERMAN, L. S. 1983 Formation of Taylor vortices in spherical Couette flow. Ph.D. thesis, Massachusetts Institute of Technology.

WERNER, B. 1984 Regular systems for bifurcation points with underlying symmetries. In *Numerical Methods of Bifurcation Problems* (ed. T. Küpper, H. D. Mittelmann & H. Weber), ISMN 70, pp. 567–574. Birkhäuser.

WERNER, B. & SPENCE, A. 1984 The computation of symmetry-breaking bifurcation points. *SIAM J. Numer. Anal.* **21**, 388–399.